Journal of Applied Polymer Science

Effects of Nickel Oxide (NiO) Nanoparticles on the Performance Characteristics of the Jatropha Oil Based Alkyd and Epoxy Blends

Pronob Gogoi, Bhaskar J. Saikia, Swapan K. Dolui
Department of Chemical Sciences, Tezpur University, Napaam, Assam 784028, India
Correspondence to: Swapan K. Dolui (E-mail: swapandolui@gmail.com)

ABSTRACT: Plant oil based alkyd resin was prepared from jatropha oil and blended with epoxy resin. Subsequently, alkyd/epoxy/NiO nanocomposites with different wt % of NiO nanoparticles have been prepared by mechanical mixing of the designed components. The structure, morphology, and performance characteristics of the nanocomposites were studied by UV-visible spectroscopy, Fourier transform infrared (FTIR) spectroscopy, scanning electron microscopy (SEM), transmission electron microscopy (TEM), X-ray diffraction (XRD), thermogravimetric analysis (TGA), differential scanning calorimetry (DSC), and universal testing machine (UTM). The alkyd/epoxy/NiO nanocomposites showed the gradual increase in thermal stability with increasing NiO content. With 3 wt % NiO content the tensile strength of the nanocomposite increased by 19 MPa (more than twofold) when compared with the pristine polymer. Limiting oxygen index (LOI) value of the nanocomposites indicate that the incorporation of NiO nanoparticles even in 1 wt % can greatly improves the flame retardant property of the nanocomposites. This study confirms the strong influence of NiO nanoparticles on the thermal, mechanical, and flame retardant properties of the alkyd/epoxy/NiO nanocomposites. © 2014 Wiley Periodicals, Inc. J. Appl. Polym. Sci. **2015**, *132*, 41490.

KEYWORDS: blends; composites; flame retardance; polyesters; thermal properties

Received 3 July 2014; accepted 4 September 2014
DOI: 10.1002/app.41490

INTRODUCTION

In recent time, the use of petroleum resources in manufacturing of different industrial products is facing some serious troubles. This is the result of more environmentally aware consumer society, high rate of depletion of petroleum resources, and spiraling rise in prices of nonrenewable stocks.[1–3] Therefore, development of polymers from renewable resources has received a great scientific attention. Amongst different renewable resources, plant oils have attracted much attention as raw materials for the chemical industry and are widely used for the surfactants, cosmetic products, and lubricants and also in coatings and paints application. Vegetable oils have been utilized in the synthesis of various polymeric resins, such as, polyester,[4] epoxy,[5] poly(urethane),[6] and poly(ester amide).[7]

Among the various products of vegetable oils, alkyd resins are most widely used in paints industries. Alkyd resins also find extensive applications in surface-coating, adhesive and composite materials, and so on.[8] However, some major drawbacks of the vegetable oil based alkyd resins, such as low mechanical strength, low hardness, low thermal stability, and long curing time limits their practical application. To overcome these drawbacks, alkyd resins were blended with other suitable resins, such as epoxy resin, amino resin, silicone resin, and ketonic resin.[9]

Dutta et al. reported the preparation of alkyd/epoxy blends as multipurpose coatings. The alkyd/epoxy blends showed better performance in terms of drying time, hardness, flexibility, gloss, thermal stability, and chemical resistance.[10] Wang et al. reported the development of alkyd/acrylic blends for the creation of hard coatings. However, alkyd resin and acrylic phase was found to be more compatible in alkyd/acrylic hybrid latex than the alkyd/acrylic blends.[11] Radicevic and Simendic reported the preparation of alkyd/melamine resin blends with various ratio of melamine. It was observed that the degree of curing alkyd/melamine resin blends increases with increasing the ratio of melamine in the blends.[12] Pasari and Chandra reported blends of polystyrene glycol and alkyd resins. The polystyrene glycol and alkyd blends were superior in film properties to the alkyd resin except in solvent resistant property.[13]

Polymer nanocomposites based on multifunctional nanoparticles, such as metal oxides, silicates, fullerenes, carbon nanotubes, graphene, and expanded graphite are being developed. The nanoparticles have strong impact on thermal, mechanical, electrical barrier, and flame retardant properties of the nanocomposites.[14,15] Lligadas et al. reported the preparation of epoxidized linseed oil/polyhedral oligomeric silsesquioxanes nanocomposites. Substantial improvement in polymeric

Table I. Mass (g) of Each Reagent Used in the Nanocomposite Formulations

Entry	Alkyd	MEKP	Co-octoate	Epoxy	Poly(amido amine)	NiO (wt %)
1	3	0.12	0.06	3	1.5	0
2	3	0.12	0.06	3	1.5	1
3	3	0.12	0.06	3	1.5	2
4	3	0.12	0.06	3	1.5	3

properties including thermal stability, mechanical strength and flame retardant were observed in the nanocomposites.[16] Xia and Larock reported the preparation of waterborne castor oil-based polyurethane–silica nanocomposites prepared through a sol–gel process. The silica nanoparticle not only reinforces the resulting coatings but also increases the crosslink density of the nanocomposites. The nanoparticles play an important role in improving the thermal and mechanical properties of the resulting nanocomposites.[17] In our previous work, we reported the preparation of jatropha oil based alkyd/epoxy composites, reinforced with expanded graphite (EG) by mechanical mixing of the designed components. The composites exhibited quite impressive properties in terms of thermal, mechanical, flame retardancy, water absorption, and *in vitro* degradation.[9] Polymers that are biodegradable and derived from renewable resources are moving into the mainstream and can compete with commodity polymers. Moreover, reinforcement of the bio-based polymers with nanofiller can produce new value-added "green" nanocomposites in the materials world.

As the incorporation of NiO nanoparticles into the polymer matrix significantly improves the electrical, thermal, and mechanical properties of the resulting nanocomposite, the synthesized NiO nanoparticles may greatly favor the performance enhancement of alkyd/epoxy blends in surface coating applications. Moreover, there is no report on the study of flame retardant property of NiO based nanocomposites. Inspiring from these studies, the objective of our current work is to fabricate nanocomposites films that contain reinforcing NiO nanofillers in an alkyd/epoxy blend matrix. For the first time we are reporting the fabrication of bio-based polymer/NiO nanocomposites. The performance characteristics including, scratch hardness, chemical resistance, thermal, mechanical and flame retardant properties of the nanocomposites were investigated with different wt % of NiO.

EXPERIMENTAL

Materials and Methods

$NiCl_2.6H_2O$, $NaHCO_3$, PbO, and phthalic anhydride of analytical grade were purchased from Merck, India. Epoxy resin (Epoxy equivalent weight: 170–180 g/eq) and hardener poly(amido amine), methyl ethyl ketone peroxide (MEKP), and Co-octoate of commercial grade were purchased from Kumud Enterprises, Kharagpur, West Bengal, India. All the materials were used as received without any further purification. Jatropha seed was collected from Sonitpur, Assam, India and the oil was extracted with petroleum ether in a soxhlet extractor. Crude oil was purified by column chromatography over silica gel using a mixture of 98% petroleum ether and 2% ethyl acetate as eluent. The average molecular weight of the oil was found to be 883 with PDI 1.05.

Synthesis of Alkyd Resins from Jatropha Oil

Alkyd resin was synthesized by a two-step method from jatropha oil. The first step was the alcoholysis process in which monoglyceride of jatropha oil was prepared by reaction of jatropha oil with glycerol in a 1 : 2 mol ratio at 210°C using lead monoxide as catalyst (0.05 wt % with respect to oil). The progress of the reaction was monitored by checking its solubility in methanol (1 : 3 v/v). The reaction was stopped when the reaction product was completely soluble in methanol at room temperature.

In the second step, the esterification reaction was carried out between monoglyceride and phthalic anhydride (0.12 mol) at 220°C and the reaction was continued until it reached acid value in the range of 10–20.[4]

Synthesis of NiO Nanoparticles

Defect free, single crystalline NiO nanoparticles were synthesized by a two-step chemical synthesis route.[18] In a typical method $NiCl_2.6H_2O$ (2.4 g) and $NaHCO_3$ (1.2 g) were dissolved in distilled water (10 mL) separately in conical flask. The $NiCl_2.6H_2O$ solution was stirred for 15 min and under constant stirring $NaHCO_3$ solution was added drop wise at room temperature. The reaction was stopped when the gas formation was ceased from the reaction mixture. The resultant product was collected by centrifugation and washed thoroughly with distilled water. The collected product was dried at 100°C in an oven and then reheated at 600°C for 2 h in a muffle furnace. The plausible reaction mechanism of the formation of NiO nanoparticles are shown below:

$$Ni^{2+}(aq) + 2HCO_3^-(aq) \xrightarrow{H_2O} Ni(HCO_3)_2.nH_2O\ (s)$$

$$Ni(HCO_3)_2.nH_2O\ (s) \xrightarrow{100^\circ C} Ni(HCO_3)_2(s) + nH_2O\ (g)$$

$$Ni(HCO_3)_2(s) \xrightarrow{600^\circ C} NiO\ (s) + 2CO_2(g) + H_2O\ (g)$$

Preparation of the Alkyd/Epoxy/NiO Nanocomposites

The alkyd/epoxy/NiO nanocomposite was prepared by solution blending method. The alkyd and epoxy was blended at the ratio of 1 : 1 in acetone (1 mg/mL) and then NiO was added in different wt % (Table I). The mixture was stirred by mechanical stirrer followed by ultrasonication for 1.5 h to get homogeneous dispersion of the NiO nanoparticles within the polymer matrix. The solvent was evaporated at 55°C and the mixture was dried

at 40°C in a vacuum oven until it was completely bubble free. Afterward, poly (amido amine) (50 wt % with respect to the epoxy resin) along with MEKP and Co-octoate (4 and 2 wt %, respectively, with respect to the alkyd resin) were added to the mixture. The mixture was then placed on a teflon sheet by an applicator maintaining the film thickness of 5 mm and dried under vacuum in a desicator for overnight at ambient temperature. The nanocomposites were allowed to cure at 80°C for further study.

Characterization Techniques

The UV-visible absorption spectra of the samples were recorded in the range of 200–700 nm by using Shimadzu UV-2550 UV-visible spectrophotometer at room temperature. Fourier-transform infrared (FTIR) spectra were recorded on a Nicolet, Impact 410 FTIR spectrometer at room temperature over a frequency range of 4000–400 cm^{-1}. The crystalline structure of NiO nanoparticles and the nanocomposites were studied by using a X-ray diffractometer (Miniflex, Rigaku Japan) with Cu Kα radiation ($\lambda = 0.154$ nm) at 30 kV and scanning rate of 0.005 s^{-1} in a 2θ range of 10°–70°. To study the thermal degradation of the nanocomposites, thermogravimetric analysis (TGA) was carried out on a Shimazdu TGA 50, thermal analyzer in nitrogen atmosphere at a heating rate of 10°C min^{-1} in the temperature range of 25–600°C. The glass transition and crystallization behaviors were investigated by differential scanning calorimetry using a Shimadzu DSC-60 in nitrogen atmosphere. The analysis was run at a scanning speed of 10°C min^{-1} from 25 to 200°C. The surface morphology of the specimens was studied by scanning electron microscope (SEM) of model JSM-6390LV, JEOL, Japan at an accelerating voltage of 5–15 kV. The surface of the specimens was coated with platinum before the SEM analysis. The dispersion and particle size of NiO nanoparticles were studied by transmission electron microscope (TEM, JEOL JEM 2100) at an acceleration voltage of 200 kV. The tensile strength, elongation, and elastic modulus of the nanocomposites were measured on a universal testing machine (Zwick Z010, Germany) at ambient conditions. The extension rate was 5 mm/min and the load cell was 10-kN, with a gauge length of 40 mm. The specimen dimension was 60 mm in length, 10 mm in width, and 0.3 mm in thickness. Three parallel measurements were carried out for each sample. Scratch hardness test on the cured films was carried out by a scratch hardness tester (Sheen instrument Ltd., UK). The chemical resistance test was done to study the effect of chemicals, such as water, ethanol (25%, aq.), NaOH (2%, aq.), and HCl (10%, aq.) on the nanocomposites. Small pieces of the nanocomposite films were kept in the aforesaid medium in 100 mL amber glass bottles at 30°C. The percent weight loss of the films was measured after 21 days of test. To study the flammability property of the nanocomposites the limiting oxygen index (LOI) was recorded in a flammability tester (S.C. Dey and Co., Kolkata). The samples were cut into 100 mm × 6 mm × 3 mm (longitudinal × tangential × radial) according to ASTM-D 2863 and placed vertically in the flammability tester. The ratio of N_2 and O_2 at which the sample continued to burn was recorded for at least 30 s.

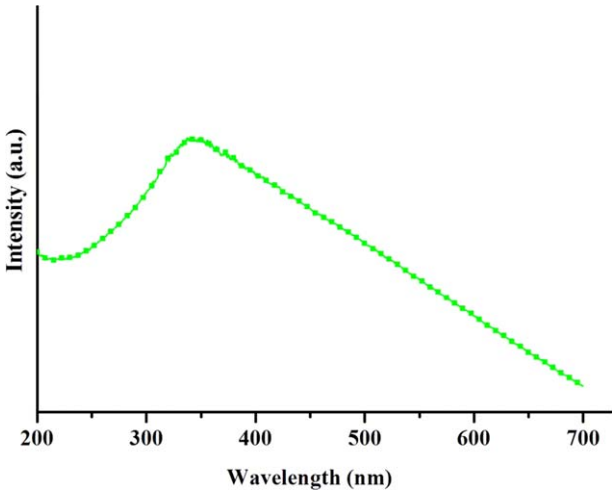

Figure 1. UV-visible spectra of synthesized NiO nanoparticles. [Color figure can be viewed in the online issue, which is available at wileyonlinelibrary.com.]

$$\text{LOI } (\%) = \frac{\text{Volume of } O_2}{\text{Volume of } O_2 + \text{Volume of } N_2} \times 100$$

RESULTS AND DISCUSSIONS

UV-Visible Study

The UV-visible study was done to investigate the formation of NiO nanoparticles and the spectrum is shown in Figure 1. The UV-visible spectrum of NiO nanoparticles showed a maximum absorption band at 343 nm (3.61 eV) due to the surface plasmon absorption of NiO nanoparticles. This type of resonance is observed when the wavelength of the incident light far exceeds the particle diameter. Thus, the maximum absorption band at 343 nm in UV-visible spectrum indicates the formation of NiO nanoparticles.[19]

FTIR Spectroscopic Analysis

The FTIR transmittance spectra of alkyd/epoxy, NiO and alkyd/epoxy/NiO nanocomposite is shown in Figure 2. FTIR spectra of the alkyd/epoxy blend [Figure 2(a)] shows bands at 2920 and 2840 cm^{-1} corresponds to the C-H stretching vibration. The bands at 1270 and 1053 cm^{-1} can be attributed to the in-plane vibration of =C–H bond. The bands at 1636 and 1753 cm^{-1} refer to C=C (belonging to fatty acid chain of monoglyceride) and C=O stretching vibration (belonging to ester group of monoglyceride), respectively. The bands observed at 1430 and 1060 cm^{-1} are, respectively, assigned to O-C=O symmetric and C-O stretching vibration. The –OH stretching vibration band appears at 3410 cm^{-1}.[20,21] In the FTIR spectra of NiO [Figure 2(b)] the bands centered at 3490 cm^{-1} and 1583 cm^{-1} correspond to asymmetric stretching and bending vibration of water, respectively. It can be attributed to the fact that the NiO nanoparticles tend to physically absorb water. The band at 451 cm^{-1} is attributed to the Ni-O stretching of the NiO nanocrystals.[22] In the FTIR spectra of alkyd/epoxy/NiO nanocomposites [Figure 2(c)] mostly all the stretching frequencies are same as that of neat NiO and alkyd/epoxy blend. However, a slight shifting of Ni-O stretching vibration frequency occurs at 487 cm^{-1} [Figure 2(c)] because of the binding of NiO nanoparticles to the

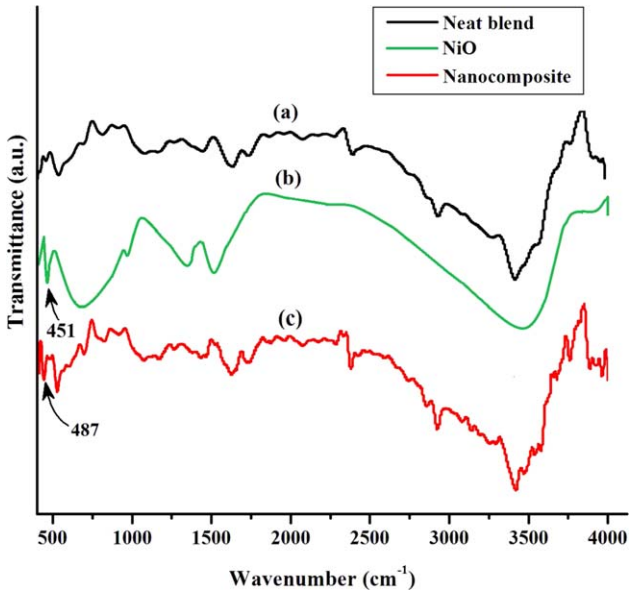

Figure 2. FT-IR spectra of (a) neat blend, (b) neat NiO and (c) nanocomposites. [Color figure can be viewed in the online issue, which is available at wileyonlinelibrary.com.]

polymer matrix. The result strongly suggests the interaction between NiO nanoparticles and the alkyd/epoxy blend matrix.[23]

Surface Morphology Analysis

The size, distribution, and morphology of the nanoparticles were characterized by SEM and TEM study. Figure 3 represents the SEM micrographs of the neat NiO and alkyd/epoxy/NiO nanocomposites. The NiO nanoparticles are spherical in shape with an average diameter of 20 nm. The SEM micrograph shows the homogeneous distribution of the nanoparticles within the alkyd/epoxy blend matrix. The SEM study also reveals the smooth and uniform surface morphology of the NiO nanoparticles. It is obvious that the NiO nanoparticles retain their shape and crystalline structure in the nanocomposites [Figure 3(b)].

The TEM micrographs of NiO and alkyd/epoxy/NiO nanocomposites are presented in Figure 4. The synthesized NiO nanoparticles have an average diameter of 15–20 nm with narrow size distribution (mean diameter about 5 nm). Well-defined nanocrystalline morphology of the NiO nanoparticles can be seen from the TEM study [Figure 4(b)].[24] TEM study also reveals the spherical particle shape with smooth and uniform morphology of the NiO nanoparticles. No agglomeration of the NiO nanoparticles is observed. From the micrographs it is clear that the NiO nanoparticles are homogeneously dispersed within the alkyd/epoxy blend matrix [Figure 4(c, d)].

XRD Analysis

The XRD patterns of alkyd/epoxy, NiO and alkyd/epoxy/NiO (1–3 wt %) nanocomposites are shown in Figure 5. The XRD pattern of alkyd/epoxy blend exhibits a weak and broad peak at $2\theta = 19.85°$ indicating that the blend is amorphous in nature [Figure 5(a)]. In the XRD pattern of NiO [Figure 5(e)] the appearance of the peaks at $2\theta = 37.30°$ (111), 43.35° (200), 62.95° (220), 75.45° (311), and 79.35° (222) confirmed the formation of NiO nanoparticles.[19] The sharpness and the intensity of the peaks indicate the crystalline nature of the synthesized NiO nanoparticles. It is noticeable that maximum NiO crystallite growth occurs along (200) the plane. In the XRD patterns of the alkyd/epoxy/NiO (1–3 wt %) nanocomposites [Figure 5(b–d)] the occurrence of the peaks at $2\theta = 37.30°$, 43.35°, 62.95°, 75.45°, and 79.35° revealed the existence of NiO nanoparticles in the designed nanocomposites. The broad peak for the alkyd/epoxy blend ($2\theta = 19.85°$) also observable in the XRD pattern of the nanocomposites. The intensity of the peaks for the NiO nanoparticles in the alkyd/epoxy/NiO nanocomposites is observed to be increased gradually with increasing NiO wt %. It can be explained by the fact that higher the wt % of NiO nanoparticles, higher is the number of NiO crystallites in the nanocomposites.[25]

The average crystallite sizes of NiO and alkyd/epoxy/NiO (1–3%) nanocomposites for the prominent peaks (111), (200), and (220) are calculated employing Debye–Scherrer's relation.[26]

$$D = k\lambda/\beta \cos\theta \quad (1)$$

where D is the average crystallite size, k is an empirical constant equal to 0.89, λ is the wavelength of the X-ray source

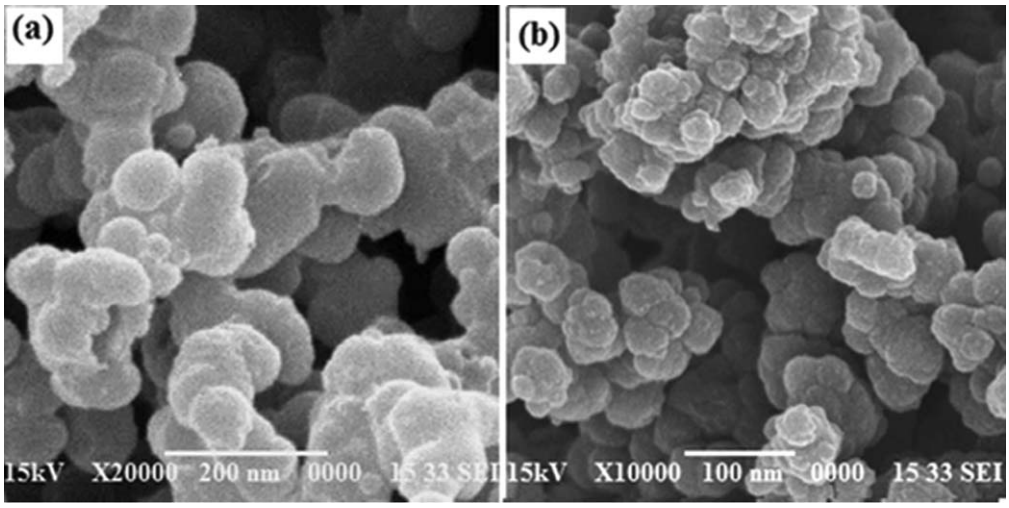

Figure 3. SEM micrographs of (a) neat NiO and (b) alkyd/epoxy/NiO nanocomposite.

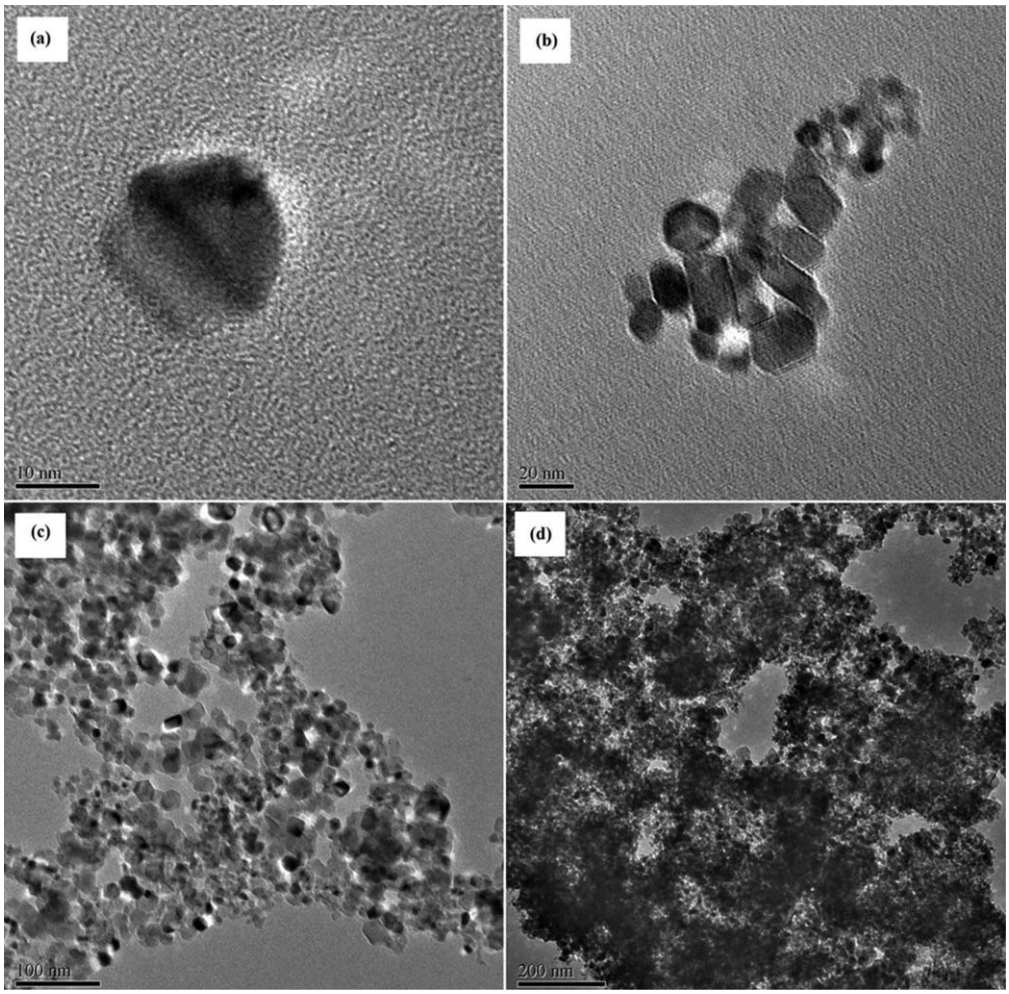

Figure 4. TEM micrographs of NiO (a and b) and alkyd/epoxy/NiO nanocomposites (c and d).

(0.15405 nm), β is the full width at half maximum of the peak, and θ is the angular position of the peak. From eq. (1), the average crystallite size of NiO nanoparticles is found to be 25.35 nm, which is in good agreement with the TEM results (15–20 nm). For the alkyd/epoxy/NiO (1–3%) the crystallite size of NiO nanoparticles do not change to a noticeable extent. It implies that the crystallinity of NiO is not disturbed by the interaction with the alkyd/epoxy blend matrix. It is also clearly observed in the TEM micrographs of the nanocomposites.[27]

Thermal Analysis

TGA Study. Figure 6 shows TGA weight loss and weight loss derivative curves for the nanocomposite films in nitrogen atmosphere. The degradation at temperatures between 250°C and 415°C can be attributed to the decomposition of aliphatic moieties of the epoxy resin and the poly(amido amine) hardener. The degradation observed in the temperature range from 430°C to 520°C resulted from chain scission in the jatropha oil and aromatic moiety of alkyd resin.[28] The TGA data such as initial degradation temperature (T_i), decomposition temperature at different at weight losses (T_d), maximum pyrolysis temperature (T_m), and residual weight are summarized in Table II. Significant improvement in thermal stability of the nanocomposite is observed by the incorporation of NiO nanoparticles. The T_i for the neat polymer is 284°C, whereas the same for the nanocomposite containing 3 wt % NiO is improved by 41°C. Even with 1 wt % of NiO the initial degradation temperature of the nanocomposite increased by 11°C and increases linearly with increasing NiO concentration. This can be attributed to the heat shielding effect of NiO. The homogeneous dispersion of the nanoparticles within the polymer matrix provides a thermal barrier, releasing combustible volatiles during decomposition. Higher the concentration of NiO nanoparticles, higher is the insulating effect. Similar results were observed for the nanocomposites reinforced with nano Al_2O_3 and TiO_2.[29,30] Moreover, the decomposition of polymers starts with the free radical formation at the weak bonds and/or chains ends, followed by radical transfer to adjacent chains through inter chain reactions. The homogeneous dispersion and strong interfacial interaction between the NiO and the polymer matrix reduces the polymer chain mobility in the nanocomposites and thereby the chain transfer reaction is suppressed and consequently the degradation process is delayed.[31]

It is observed from Table II that decomposition temperature at different weight losses and T_{max} for all of the nanocomposites increase with an increase in the NiO content. This can be explained by the fact that the incorporation of NiO

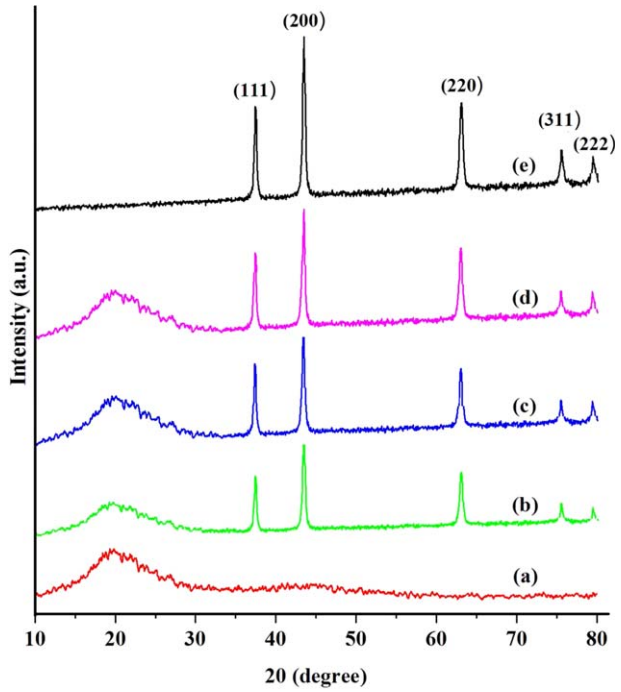

Figure 5. XRD patterns of (a) alkyd/epoxy blend, (b) nanocomposite (1% NiO), (c) nanocomposite (2% NiO), (d) nanocomposite (3% NiO), and (e) neat NiO. [Color figure can be viewed in the online issue, which is available at wileyonlinelibrary.com.]

nanoparticles within the polymer matrix creates an inert and impermeable layer to the volatile products generated during degradation process and improve the thermal stability of the nanocomposites.[30]

DSC Study. Figure 7 represents the DSC thermograms for the nanocomposite films with different NiO concentrations. Neither melting nor crystallization transitions were observed in the DSC curves, indicating the amorphous nature of the nanocomposites. However, the glass transition temperature (T_g) is clearly seen for all the nanocomposites in the temperature range of 55–75°C. For the alkyd/epoxy blend T_g is found to be 56°C, whereas the incorporation of NiO significantly improved the T_g of the nanocomposites. The T_g increases linearly with increasing NiO content and found to be increased by 20°C for the nanocomposite with 3% NiO when compared with the neat polymer. It can be explained by the reduced mobility of the polymer

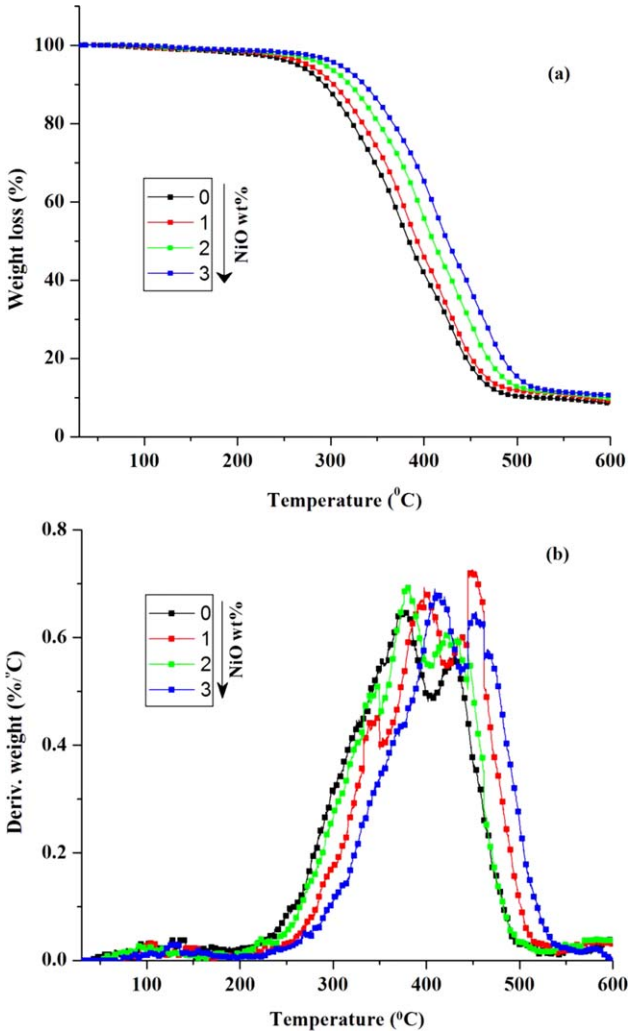

Figure 6. TGA thermograms (a) and their derivative curves (b) of the nanocomposites. [Color figure can be viewed in the online issue, which is available at wileyonlinelibrary.com.]

chain in the presence of NiO nanoparticles. These results clearly suggest strong interaction (dipole–dipole) between NiO nanoparticles and the polymer matrix. Moreover, the homogeneous dispersion of the nanoparticles within the polymer matrix efficiently restricts the segmental motion of the polymer chains on the interface.[32]

Table II. Thermal Degradation Data and LOI (%) of the Nanocomposites

		Decomposition temperature (T_d, °C) at different wt losses						
NiO wt %	T_i (°C)	$T_{10\%}$	$T_{30\%}$	$T_{50\%}$	$T_{70\%}$	T_m (°C)	Residue (%) at 600 °C	LOI (%)
0	284	293	347	384	425	374	8	20 (± 0.83)
1	294	304	359	393	431	380	9	27 (± 0.26)
2	309	320	376	410	449	400	10	34 (± 0.47)
3	325	335	391	426	464	415	11	42 (± 0.63)

T_i = Initial degradation temperature; T_m = maximum pyrolysis temperature.

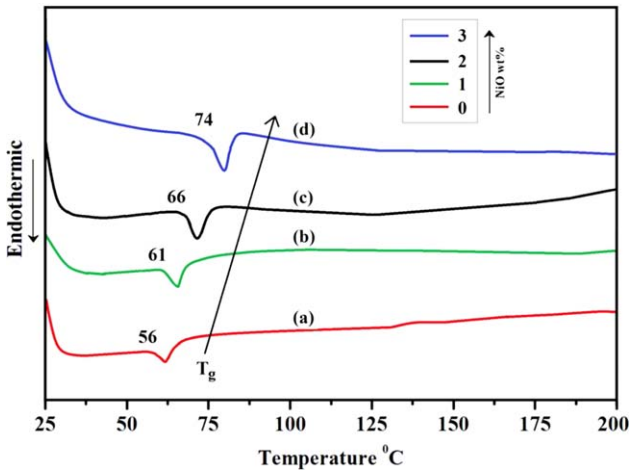

Figure 7. DSC traces of (a) alkyd/epoxy blend, (b) nanocomposite (1% NiO), (c) nanocomposite (2% NiO), (d) nanocomposite (3% NiO). [Color figure can be viewed in the online issue, which is available at wileyonlinelibrary.com.]

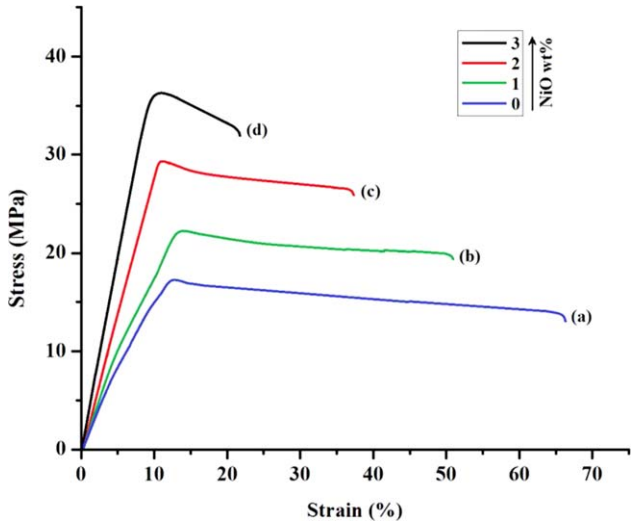

Figure 8. Stress–strain curves for the nanocomposites. [Color figure can be viewed in the online issue, which is available at wileyonlinelibrary.com.]

Mechanical Properties. NiO nano filler is expected to have good reinforcement effect on mechanical properties of nanocomposites because of its high aspect ratio. The performance of the alkyd/epoxy blend effectively changed with the incorporation of NiO nanoparticles. Mechanical properties like tensile strength, elongation at break (%), Young's modulus, and toughness of the nanocomposite films are summarized in Table III. The tensile stress–strain curves for the nanocomposite films with different wt % of NiO are shown in Figure 8. As expected, NiO acts as genuine nanofiller on the mechanical properties of polymer nanocomposites. Tensile strength and elastic modulus of the nanocomposites increases linearly with increasing NiO concentration. With 3% NiO the tensile strength and elastic modulus of the alkyd/epoxy/NiO nanocomposite improved by 211% and 173%, respectively. It implies the sufficient transfer of mechanical energy from polymer matrix to the nanofiller. The mechanical energy transfer is only plausible when the nanofiller is strongly attached to the polymer matrix.[33,34] The homogeneous dispersion of the nanoparticles also reinforces effect. However, as a result of the strong interaction between the NiO nanoparticles and alkyd/epoxy blend matrix reduces the mobility of the polymer chain. This also reflects in the decreased elongation at break (%) of the alkyd/epoxy/NiO nanocomposites when compared with the neat alkyd/epoxy blend. The nanocomposite with 2 wt % NiO exhibited the best toughness (928) as it possesses overall good tensile strength (29 MPa) and elongation at break (37%). The increment in scratch hardness of the nanocomposites with the NiO content can be attributed to the enhanced strength of the nanoreinforcing NiO nanoparticles and flexibility of the long hydrocarbon chains of the fatty acid part of the alkyd resin.

Limiting Oxygen Index (LOI). The LOI values of the neat polymer and the nanocomposites with different weight ratios of NiO nanoparticles are summarized in Table II. It is observed that the pristine blend showed a LOI value of 20%. The neat polymer essentially composed of hydrocarbon chains; as a consequence it requires very less amount of oxygen for the propagation of flame, and therefore, showed low flame retardancy.[9] The incorporation of NiO nanoparticles significantly improves the flame retardancy of the nanocomposites. The LOI value of the nanocomposites increases gradually with increasing NiO concentration. The addition of NiO nanoparticles promoted the char formation and thereby improves the flame retardancy of the nanocomposites by insulating the surface of the composites. Moreover, the nanofiller rich composite surface has better barrier properties to heat and oxygen transport, which delays the ignition of the nanocomposites.[35,36] Higher the concentration of NiO nanoparticles, higher is the char formation and hence higher will be the LOI value.

Chemical Resistance. The chemical resistance test of the thermosets are carried out in water, NaOH (1%, aq.), HCl (10%,

Table III. Mechanical Properties of the Nanocomposites

Entry	NiO wt %	Tensile strength (MPa)	Elastic modulus (GPa)	Elongation at break (%)	Toughness	Scratch hardness (kg)[a]
1	0	17 ± 0.42	1.26 ± 0.31	67 ± 2	825	8.3
2	1	22 ± 0.13	1.81 ± 0.43	51 ± 2	880	9.4
3	2	29 ± 0.25	1.98 ± 0.16	37 ± 2	928	>10
4	3	36 ± 0.27	2.18 ± 0.18	21 ± 2	510	>10

[a] Limit of the instrument for scratch hardness was 10.0 kg (max).

Table IV. Chemical Resistance (wt loss %) of the Thermosets in Different Chemical Environments

		Chemical environment			
Entry	NiO wt %	Water	Ethanol (25%, aq.)	NaOH (2%, aq.)	HCl (10%, aq.)
1	0	0	0	2.47	2.63
2	1	0	0	1.09	1.45
3	2	0	0	0.54	1.26
4	3	0	0	0.21	0.86

aq.), and ethanol (20%, aq.) and the results are summarized in Table IV. The nanocomposites exhibited excellent solvent and good acid and alkali resistance. This is due to the highly cross-linked and condensed/rigid structure of the nanocomposites. The weight loss (%) decreases with increasing NiO concentration in the nanocomposites. This is due to the increasing compactness of the nanocomposite structure with increasing NiO wt %. As the polymer matrix contains hydrolysable ester linkages in the structure, the alkali resistance of the composites is relatively poor. But due to the presence of rigid aromatic moieties in the alkyd resins, the alkali resistance of the nanocomposites is yet satisfactory.

CONCLUSIONS

NiO nanoparticles was synthesized by hydrothermal method and successfully incorporated into the alkyd/epoxy blend matrix. The nanoparticles are spherical in shape with smooth surface and uniform morphology having particle diameter 15–20 nm. XRD study shows the existence of NiO nanoparticles in the alkyd/epoxy/NiO nanocomposites with well crystalline nature. Thermal stability of the nanocomposites increased noticeably by the incorporation of NiO nanoparticles. For the alkyd/epoxy/NiO (3%) nanocomposite, the initial degradation temperature increased by 41°C. With 3% NiO, the T_g of the nanocomposites enhanced by 20°C. When compared with the pristine blend, the tensile strength and elastic modulus increased by 211% and 173%, respectively, with 3% NiO. The results strongly suggest the efficient load transfer between NiO and the alkyd/epoxy blend matrix. The NiO nanoparticle has a significant effect on the flame retardant property of the nanocomposites. LOI value of the alkyd/epoxy/NiO increased up to 42% with 3% NiO. The alkyd/epoxy/NiO nanocomposites exhibited good resistance toward solvent, acid, and alkali solution. All the results form the analyses deduce a conclusion that the NiO nanoparticles have significant effects on the performance characteristics of the alkyd/epoxy blends. The use of renewable raw materials can reinforce the rapid development of sustainable and eco-friendly materials to the environmentally aware consumer society.

ACKNOWLEDGMENTS

The authors express their gratitude and thanks to the authority of Tezpur University for providing facility to carry out this work. One of the authors (P. Gogoi) is grateful to the UGC, India, for providing Junior Research Fellowship as a financial support to carry out the research work.

REFERENCES

1. Ahmed, S.; Ashraf, S. M.; Naqvi, F.; Yadav, S.; Hasnat, A. *Prog. Org. Coat.* **2003**, *47*, 95.
2. Kundu, P. P.; Larock, R. C. *Biomacromolecules* **2005**, *6*, 797.
3. Eren, T.; Kusefoglu, S. H. *J. Appl. Polym. Sci.* **2005**, *97*, 2264.
4. Boruah, M.; Gogoi, P.; Adhikari, B.; Dolui, S. K. *Prog. Org. Coat.* **2012**, *74*, 596.
5. Altuna, F. I.; Pettarin, V.; Williams, R. J. *J. Green Chem.* **2013**, *15*, 3360.
6. Hablot, E.; Zheng, D.; Bouquey, M.; Averous, L. *Macromol. Mater. Eng.* **2008**, *293*, 922.
7. Ahmed, S.; Ashraf, S. M.; Yadav, S.; Jamal, A. *J. Appl. Polym. Sci.* **2001**, *82*, 1855.
8. Bora, M. M.; Gogoi, P.; Deka, D. C.; Kakati, D. K. *Ind. Crop. Prod.* **2014**, *52*, 721.
9. Gogoi, P.; Boruah, M.; Bora, C.; Dolui, S. K. *Prog. Org. Coat.* **2014**, *77*, 87.
10. Dutta, N.; Karak, N.; Dolui, S. K. *J. Appl. Polym. Sci.* **2006**, *100*, 516.
11. Wang, T.; Alarcon, C. D. L. H.; Goikoetxea, M.; Beristain, I.; Paulis, M.; Barandiaran, M. J.; Asua, J. M.; Keddie, J. L. *Langmuir* **2010**, *26*, 14323.
12. Radicevic, R. Z.; Simendic, J. K. B. *J. Serb. Chem. Soc.* **2005**, *70*, 593.
13. Pasari, M. S.; Chandra, S. *Pigm. Resin Technol.* **1979**, *8*, 12.
14. Uhla, F. M.; Yao, Q.; Nakajima, H.; Manias, E.; Wilkie, C. A. *Polym. Degrad. Stab.* **2005**, *84*, 70.
15. Dykes, L. M. C.; Torkelson, J. M.; Burghardt, W. R. *Macromolecules* **2012**, *45*, 1622.
16. Lligadas, G.; Ronda, J. C.; Galià, M.; Cádiz, V. *Biomacromolecules* **2006**, *7*, 3521.
17. Xia, Y.; Larock, R. C. *Macromol. Rapid Commun.* **2011**, *32*, 1331.
18. Chakrabarty, S.; Chatterjee, K. *J. Phys. Sci.* **2009**, *13*, 245.
19. Das, D.; Nath, B. C.; Phukon, P.; Saikia, B. J.; Kamrupi, I. R.; Dolui, S. K. *Mater. Chem. Phys.* **2013**, *142*, 61.
20. Pathan, S.; Ahmad, S. *ACS Sustain. Chem. Eng.* **2013**, *1*, 1246.
21. Allauddin, S.; Narayan, R.; Raju, K. V. S. N. *ACS Sustain. Chem. Eng.* **2013**, *1*, 910.
22. Mayya, K. M.; Jain, N.; Gole, A.; Langevin, D.; Sastry, M. *J. Colloid Interf. Sci.* **2004**, *270*, 133.
23. Sonavane, A. C.; Inamdar, A. I.; Dalavi, D. S.; Deshmukh, H. P.; Patil, P. S. *Electrochim. Acta* **2010**, *55*, 2344.
24. Nalage, S. R.; Chougule, M. A.; Sen, S.; Patil, V. B. *J. Mater. Sci. Mater. Electron.* **2013**, *24*, 368.
25. Chen, G.; Wu, D.; Weng, W.; Wu, C. *Carbon* **2003**, *41*, 619.
26. Cullity, B. Elements of X-ray Diffraction, A.W.R.C. Inc.: Massachusetts, **1967**.
27. Nalage, S. R.; Navale, S. T.; Patil, V. B. *Measurement* **2013**, *46*, 3268.
28. Zhang, C.; Xia, Y.; Chen, R.; Huh, S.; Johnston, P. A.; Kessler, M. R. *Green Chem.* **2013**, *15*, 1477.

29. Tibiletti, L.; Longuet, C.; Ferry, L.; Coutelen, P.; Mas, A.; Robin, J. *J. Polym. Degrad. Stab.* **2011**, *96*, 67.
30. Laachachi, A.; Leroy, E.; Cochez, M.; Ferriol, M.; Lopez Cuesta, J. M. *Polym. Degrad. Stab.* **2005**, *89*, 344.
31. Mbhele, Z. H.; Salemane, M. G.; van Sittert, C. G. C. E.; Nedeljkovic, J. M.; Djokovic, V.; Luyt, A. S. *Chem. Mater.* **2003**, *15*, 5019.
32. Chen, P.; Zhang, L. *Biomacromolecules* **2006**, *7*, 1700.
33. Yasmin, A.; Daniel, I. M. *Polymer* **2004**, *45*, 8211.
34. Zhao, X.; Zhang, Q.; Chen, D. *Macromolecules* **2010**, *43*, 2357.
35. Urbanczyk, L.; Bourbigot, S.; Calberg, C.; Detrembleur, C.; Jérôme, C.; Boschini, F.; Alexandre, M. *J. Mater. Chem.* **2010**, *20*, 1567.
36. Gilman, J. W.; Jackson, C. L.; Morgan, A. B.; Harris, R. H.; Manias, E.; Giannelis, E. P.; Wuthenow, M.; Hilton, D.; Phillips, S. *Chem. Mater.* **2000**, *12*, 1866.